Dalton Transactions

Cite this: *Dalton Trans.*, 2011, **40**, 2459

www.rsc.org/dalton

PAPER

Structures, electronic properties and solid state luminescence of Cu(I) iodide complexes with 2,9-dimethyl-1,10-phenanthroline and aliphatic aminomethylphosphines or triphenylphosphine†

Radosław Starosta,*[a] Małgorzata Puchalska,[a] Joanna Cybińska,[a,b] Maciej Barys[a] and Anja V. Mudring[b]

Received 25th September 2010, Accepted 3rd December 2010
DOI: 10.1039/c0dt01284j

The luminescent complexes of triphenylphosphine and two interesting aminomethylphosphines: $P(CH_2N(CH_2CH_2)_2NCH_3)_3$ and $P(CH_2N(CH_2CH_2)_2O)_3$ with copper(I) iodide and 2,9-dimethyl-1,10-phenanthroline (dmp): [CuI(dmp)PPh_3], [CuI(dmp)$P(CH_2N(CH_2CH_2)_2NCH_3)_3$] and [CuI(phen)$P(CH_2N(CH_2CH_2)_2O)_3$] are presented in this work. These complexes were characterized in solution by means of NMR spectroscopy and their structures were crystallographically determined in the solid state. All complexes crystallize as the discrete dimers bound by π-stacking interactions between dmp rings. The coordination geometry about the Cu(I) centre is pseudo-tetrahedral showing small flattening and large rocking distortions. The investigated compounds exhibit intense orange photoluminescence in the solid state (emission peaks at r.t.: λ_{max} = 588–592 nm; τ = 1.7–2.2 and 6.4–10.0 μs; at 77 K: λ_{max} = 605–612 nm; τ = 4.8–6.5 and 32–47 μs), which is several orders higher than the luminescence of the analogous complexes with 1,10-phenanthroline (phen). Electronic and structural properties of the [CuI(dmp/phen)PR_3] complexes were characterized using DFT methods to interpret their photophysics. On the basis of TDDFT calculations the broad CT bands observed in UV-Vis spectra are interpreted as the two mixed transitions from σ(CuI) bond with a small admixture of σ(CuP) bond to π* phen or dmp ligand: (MX,MPR_3)LCT, while the emissions most probably occur from two triplet states which are in thermal equilibrium.

Introduction

Much attention has been paid to emissive copper(I) complexes of $[Cu(NN)_2]^+$ type, where NN = 1,10-phenanthroline (phen) or its derivatives.[1–8] Studies of the mixed-ligand complexes with diimines and phosphines or diphosphines ($[Cu(NN)(P)_2]^+$ or $[Cu(NN)(P_2)]^+$)[9–24] are also extensive, because of the varied photophysical properties of these complexes. Some of them exhibit efficient electroluminescence and thus are suitable for organic light-emitting diode applications.[18,22] Other complexes, like binuclear Cu(I) complexes with phosphines and diiimines[25] or the complexes of general formula $[Cu(NN)(SP)_2]^+$ (SP = phosphine sulfide or diphoshine disulfide)[26,27] also exhibit luminescent properties.

Neutral heteroleptic complexes of [CuX(NN)P] type, where X = halogen or pseudohalogen, P = phosphine and NN = diimine are much less intensively studied despite the fact that they should more easily undergo the vacuum deposition process in the preparation of electroluminescence devices. Rather limited literature data contain only luminescent properties of $[Cu_2X_2(PPh_3)_2]$ or $[CuX(P)_3]$ (X = I, Br, Cl) complexes,[28] CuI(dipyridilo[3,2,-a:2′,3′-c]phenazine)PPh_3 complex,[29] the $[Cu_2I_2(4,4'\text{-bpy})(PR_3)_2]_x$ complexes,[30] and a well theoretically described series of [Cu(NCS){$(N)_2$ or (NN)}PR_3], (N = py, NN = 2,2′-bpy or phen) complexes.[31]

Luminescent properties of copper(I) complexes, ascribed tentatively to metal-to-ligand charge-transfer transitions (MLCT), are very complicated – especially in solution. For example, a number of the ultrafast processes of electronic relaxations and structural distortions (where serious flattening is the dominant one) are observed for the $[Cu(dmp)_2]^+$ (dmp = 2,9-dimethyl-1,10-phenanthroline) complex[1,8] and emission of this compound is a complex process with at least two emitting MLCT states.[1,3,7,8,28]

Emission processes in the solid state are much simpler, however early observations indicate the presence of a mixture of excited states leading to a two-component emission in thermal equilibrium.[10] Moreover, the quantum efficiency, the shape and the position of the emission bands in the solid state can be influenced by several factors. The most important one is the π-stacking interaction of aromatic rings.[4,5,23] Recent time-resolved diffraction and theoretical studies of $[Cu(dmp)(dppe)]^+$ (dppe = 1,2-bis(diphenylphosphino)ethane)[9] showed that the geometry of

[a]*Faculty of Chemistry, University of Wrocław, ul. F. Joliot-Curie 14, 50-383, Wrocław, Poland. E-mail: starosta@wchuwr.pl*
[b]*Anorganische Chemie I-Festkörperchemie und Materialien, Ruhr-Universität Bochum, D-44780, Bochum, Germany*

† Electronic supplementary information (ESI) available: Crystal packing pictures, detailed NMR and DFT data, as well as optimized geometries for all presented compounds. CCDC reference numbers 794447–794449. For ESI and crystallographic data in CIF or other electronic format see DOI: 10.1039/c0dt01284j

this complex changes slightly upon excitation. The calculations performed for this compound indicate that the charge transfer should be labelled rather as LLCT than MLCT, but significant electron redistribution on the copper atom is also observed.

Recently we have presented the structures and electronic properties of the phosphines: $P(CH_2N(CH_2CH_2)_2NCH_3)_3$ (**1**), $P(CH_2N(CH_2CH_2)_2NCH_2CH_3)_3$ (**2**) and $P(CH_2N(CH_2CH_2)_2O)_3$ (**3**) and their copper(I) iodide complexes with 1,10-phenanthroline (**1P**, **2P** and **3P**) or 2,2′-bipyridine (**1B**, **2B** and **3B**)[32,33] showing moderate or weak luminescence in the solid state. The syntheses of these phosphines are very convenient. Like other aminomethylphosphines they can be obtained from the reaction of $P(CH_2OH)_3$ with a stoichiometric amount of a secondary amine (see refs in 32 and 33), or in a one-pot synthesis from $P(CH_2OH)_4Cl$ after the addition of any base.

We have proved that the phosphines **1**, **2** and **3**, despite very large Tolman's cone angles (θ)[34] (210°, 219° and 206° for **1**, **2** and **3** respectively[33]) show only little influence of the substituents (alkyl piperazines or morpholine) on their electronic properties. This influence is best described by S4′[35] and S4[36] parameters (Scheme 1). While θ describes simple steric demands of phosphine ligands, the S4′ describes the geometry of the bonds formed by the phosphorus atom and therefore provides some insight into its electronic properties. Values of S4′ obtained from the X-ray structures of phosphines are equal to 64.8, 64.8 and 59.8 for **1**, **2** and **3** respectively, and values of S4 are equal to 63.65, 63.66 and 63.44 for **1**, **2** and **3** respectively. It is worth mentioning that the values of both S4′ and S4 parameters of phosphines decrease dramatically upon formation of the chalcogenide derivatives, thus these parameters are good indicators of changes in the electron distribution at the phosphorus atom.[33]

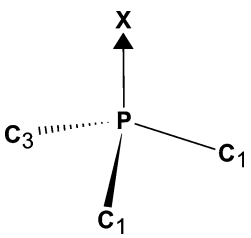

Scheme 1 Definition of the S4′ (symmetric deformation coordinate from crystallographic studies[35]) or S4 (from the *ab initio* calculations[36]) parameters. $S4' = (XPC_1+XPC_2+XPC_3) - (C_1PC_2+C_1PC_3+C_2PC_3)$, where X is a metal atom, a chalcogenide atom or a lone electron pair.

Since the structures of the phosphines **1** and **2**, as well as their electronic properties (MeSP,[37] S_{eff} and E_{eff}[36,38])[32] are very similar, we focus on the copper(I) iodide complexes with **1** or **3** and dmp in this study. We also present (for comparative purposes) an analogous complex with triphenylphosphine (**4**), which is the most popular phosphine ligand.

Results and discussion

Syntheses and NMR characterization of complexes

Reactions of the phosphines **1**, **3** or **4** with CuI and dmp in 1 : 1 : 1 molar ratios give yellow dmp complexes (***N***): $[CuI(dmp)P(CH_2N(CH_2CH_2)_2NCH_3)_3]$ (**1N**), $[CuI(dmp)P(CH_2N(CH_2CH_2)_2O)_3]$ (**3N**) and $[CuI(dmp)PPh_3]$ (**4N**) (eqn (1)).

$$CuI + dmp + PR_3 \rightarrow CuI(dmp)PR_3 \quad (1)$$

$$2CuI(dmp)PR_3 \rightleftharpoons Cu_2I_2(dmp)_2 + 2PR_3 \quad (2)$$

To prevent a possible dissociation of the phosphine ligand followed by formation of the binuclear $[Cu_2I_2(dmp)_2]$ species[11,12] (eqn (2)), the mixtures of **1**, **3** or **4** with CuI and dmp (or phen) in 2 : 1 : 1 molar ratios were prepared. After the evaporation of the solvent we have obtained stable mixtures: **1N1**, **3N3**, **4N4**, **1P1** and **3P3**, but the oily **4P4** decomposed in a short time. Pure, crystalline **1N**, **3N** and **4N** complexes were obtained from **1N1**, **3N3** and **4N4** mixtures in a slow crystallization process.

1N and **3N** complexes are soluble in most common solvents (except water and aliphatic hydrocarbons). The extremely high stability of their DMSO/water solutions in air (from the UV-Vis spectra: more than two months) must also be noted.

NMR spectra (Experimental Section and Table S1†) were measured in $CDCl_3$ at room temperature. For **1N** and **3N** complexes the signal of the phosphorus atom in the $^{31}P\{^1H\}$ spectra is a significantly broadened singlet moved from –60 ppm (chemical shift of P atom of the free phosphine ligands; see Table S1 in ESI†) to –28.5 ppm. For both the **1N1** and **3N3** mixtures two broad singlets at –29 and –60 ppm are observed, which indicates an exchange of the phosphine molecules. The observation of the signals of the P-CH_2- groups in the ^1H and $^{13}C\{^1H\}$ spectra also confirms this process. On the other hand, the coordination of **4** does not cause significant changes in the $^{31}P\{^1H\}$ spectra. Both spectra (**4N** and **4N4**) consist of a significantly broadened singlet at –6 ppm – chemical shift comparable to that of **4**. This indicates (together with the ^1H and $^{13}C\{^1H\}$ spectra) fast exchange processes and significant lability of **4** in **4N**.

The chemical shifts of the -Me groups of dmp are very sensitive to coordination processes. In the free ligand chemical shifts are equal to 2.90 ppm and are shifted downfield to 3.20 ppm (**1N** and **1N1**) and 3.23–3.24 ppm (**3N** and **3N3**), but for **4N** and **4N4** they are shifted toward higher fields: to 2.84 and 2.81 ppm, respectively.

Summarising, the comparison of the NMR spectra of **1N** and **3N** complexes with the spectra of the **4N** complex suggests that aliphatic phosphines **1** and **3** coordinate more strongly than aromatic phosphine **4**, and the character of the Cu–P is slightly different for **1** and **3** than for **4** most probably due to the strong π-accepting character of the latter.

X-ray diffraction studies

The crystal structures of **1N**, **3N** and **4N** ($\mathbf{1N}\cdot 0.46(C_6H_{12})\cdot CH_2Cl_2\cdot 2H_2O$, **3N** and $\mathbf{4N}\cdot 2CHCl_3$) are shown in Fig. 1 and Figs. S1–S6† (solvent molecules omitted for clarity). Selected structural data for **1N**, **3N** and **4N** complexes, together with the data for analogous phenanthroline complexes (***P***) are presented in Table 1.

All three ***N*** complexes crystallize as discrete centrosymmetric dimers bound by π-stacking interactions between the dmp molecules (Fig. 2). Among diverse possibilities[4,5] only one type of π-stacking interaction is observed. Distances between the dmp rings are 3.33–3.40 Å.

Table 1 Selected geometries of **1N**, **3N** and **4N** together with **1P**, **3P** and **4P**. (Bond lengths [Å], angles [°])

X-ray:	**1P** (A)[a]	**1P** (B)[a]	**3P**[a]	**4P**[b]	**1N**	**3N**	**4N**
Cu1–I1	2.615(2)	2.619(2)	2.631(1)	2.6157(6)	2.6535(11)	2.6738(7)	2.6284(9)
Cu1–N42	2.072(13)	2.085(11)	2.058(4)	2.071(3)	2.104(3)	2.1152(18)	2.090(4)
Cu1–N41	2.092(12)	2.063(13)	2.101(4)	2.111(3)	2.087(3)	2.0741(19)	2.074(4)
Cu1–P1	2.209(4)	2.197(4)	2.193(2)	2.1977(9)	2.2032(14)	2.2064(7)	2.2052(15)
av. (P1–C11,C21,C31)*	1.847(17)	1.832(16)	1.837(6)	1.829(3)	1.859(4)	1.855(2)	1.834(6)
N41–Cu1–N42	80.8(5)	81.3(5)	80.20(17)	79.93(10)	80.02(13)	79.79(7)	80.58(17)
I1–Cu1–N42	109.8(3)	107.9(3)	107.06(12)	107.06(7)	106.30(9)	104.93(5)	117.04(12)
I1–Cu1–N41	118.1(3)	108.4(4)	111.50(12)	110.97(7)	104.86(9)	103.06(5)	105.71(13)
I1–Cu1–P1	102.80(14)	103.52(14)	107.06(5)	112.70(3)	110.86(4)	108.24(3)	121.26(5)
N41–Cu1–P1	115.4(4)	131.9(4)	115.46(14)	130.43(8)	129.11(10)	131.46(5)	120.66(13)
N42–Cu1–P1	130.1(4)	121.6(3)	132.79(13)	110.68(7)	120.91(10)	124.53(5)	117.04(12)
S4′**	50.8	49.7	50.7	31.8	59.6	58.1	35.1
α	86.49	79.33	79.81	80.99	85.63	85.56	89.79
β	138.15	130.38	132.45	135.93	136.18	142.57	125.60
γ	118.34	126.82	120.47	111.35	112.96	109.32	113.15

[a] –**1P**·PhCH$_3$ and **3P**·0.5Cu$_2$I$_2$(phen)$_2$ from ref. 32. [b] CuI(1,10-phen)PPh$_3$ from ref. 39 *Average P–C bond lengths: 1.855(2) for **1**, 1.845(3) for **3** (ref. 32) and 1.831(2) for **4** (ref. 40).**S4′ = 64.8 for **1**, 59.1 for **3** (ref. 33) and 38.5 for **4** (ref. 40).

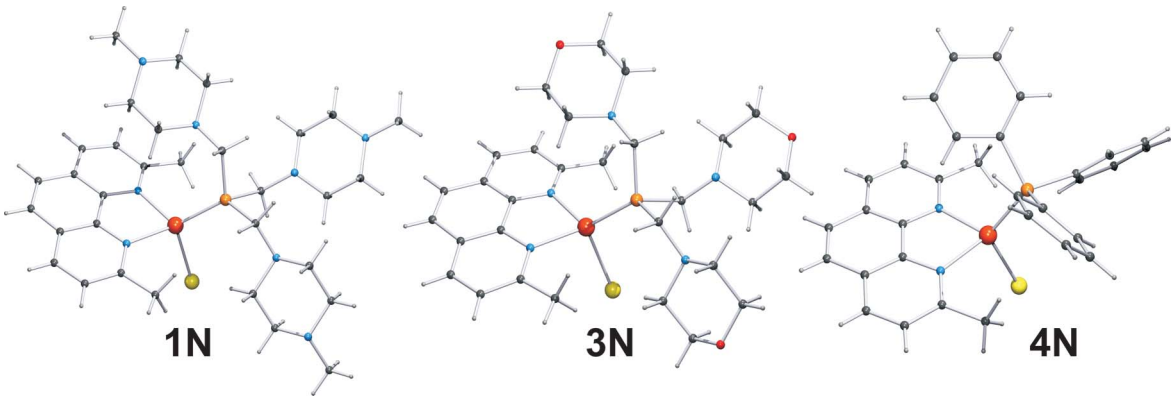

Fig. 1 View of a **1N**, **3N** and **4N** molecules in **1N**·0.46(C_6H_{12})·CH_2Cl_2·2H_2O, **3N** and **4N**·2$CHCl_3$ complexes.

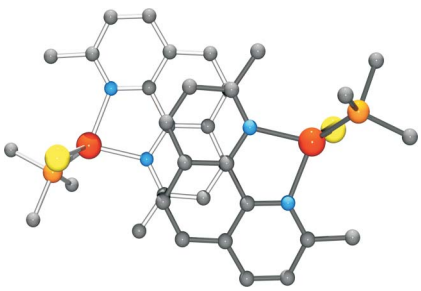

Fig. 2 π-stacking between dmp molecules in **1N**, **3N** and **4N**.

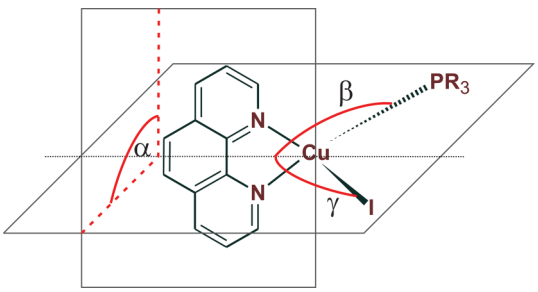

Fig. 3 Definition of structural distortions from a tetrahedral coordination sphere around copper(I) atom: α – angle between the plane of diimine and the plane of CuI and CuP bonds; β or γ – angles between the line of intersection of the former planes and CuP or CuI bond, respectively.

The coordination geometry about Cu in the ***P*** and ***N*** complexes is distorted tetrahedral. The two main distortions are: the flattening (Fig. 3 – α angle) and the rocking (Fig. 3 – the difference between β and γ angles). Flattening distortions in the ***N*** complexes are rather small: the α angles (Table 1) are equal to 85.6° for **1N** and **3N** and 89.8° for **4N**. For the ***P*** complexes the flattening distortions are definitely larger: 86.5 and 79.3° for **1P**, 79.3° for **3P** and 81.0° for **4P**.[39] The γ angles are significantly smaller than the β angles for all the compounds due to an undoubted difference in the steric demands of phosphine and iodide ligands (Table 1). Bond lengths around Cu in the ***N*** complexes do not differ significantly from those in the ***P*** complexes, the only exception are the Cu–I bond lengths, which are significantly shorter for the latter ones (Table 1).

The smallest difference in the lengths of the Cu–I bond found for **4N** and **4P** molecules suggests that the parameters of this bond are mostly influenced by steric factors, because **4** exhibits much smaller steric hindrance than **1** and **3**.

Formation of the complex obviously generates large changes in the geometries of the phosphine ligands, which are different for the ***N*** and ***P*** complexes: coordination of the phosphines causes

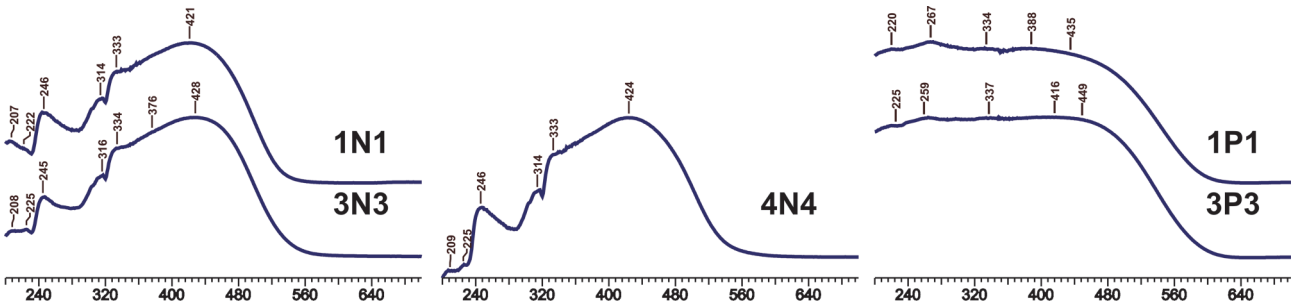

Fig. 4 UV-Vis (reflectance) spectra of solid samples at room temperature.

significant shortening of the P–C bonds for ***P*** complexes and a slight lengthening for the ***N*** ones (Table 1). Simultaneously, the S4′ parameter values (Table 1) are considerably less decreased in the ***N*** complexes than in the ***P*** ones. These differences certainly result from the presence of the methyl substituents in the dmp ligand, which considerably delimit the available space around the copper central atom.

Solid state optical properties of copper(I) complexes

UV-vis solid-state absorption (reflectance) spectra of the compounds under investigation (**1N1**, **3N3**, **4N4**, **1P1** and **3P3**) were recorded at room temperature. In contrast to the spectra of the ***P*** complexes, which are rather shapeless (absorption band starts at around 600 nm and after reaching a maximum at 450 nm remains rather constant; see Fig. 4 and ref. 32) the spectra of the ***N*** complexes exhibit several well resolved bands. Absorbance bands start at around 550 nm and reach a distinct maximum at 420–430 nm with a saddle at around 370 nm. The width and intensity of these bands clearly indicate their CT character. The next bands (333–334, 314–316, 245–246, 225–222 and 209–208 nm) may come from iodide (the first absorption band for solid state CuI or KI is located around 400 nm), phosphine or dmp ligands. The spectrum of **4N4** does not differ much from the spectra of **1N1** and **3N3**, despite the aromatic character of **4**.

All three ***N*** complexes in the solid state emit orange light. The intensity of their luminescence is several orders higher than the intensity of the luminescence of the analogous ***P*** complexes,[32] A slightly higher intensity of the luminescence of **4N4** compared to **1N1** (or **1N**) and **3N3** (or **3N**) is also noticeable. Similar π-stacking interactions found in **1N**, **3N** and **4N** let us eliminate their influence on the spectroscopic properties of the complexes under investigation.[4,5,23] The emission data are summarised in Table 2.

The luminescence spectra (r.t.) show a broad band characteristic for the CT transitions (Fig. 5). The shapes and positions of the bands are approximately identical within **XN–XNX** and **XP–XPX** and do not depend on the excitation wavelength (450–275 nm). The excitation spectra (Fig. 6) measured for the emission maxima show at least 3–4 bands and are similar to the reflectance spectra in the initial (600–420 nm) range. The maximum of the emission band of the ***N*** complexes is hipsochromically shifted by approximately 60 nm in comparison to the ***P*** complexes. Some differences in spectra parameters within the **1P–1P1** pair are most probably the result of the lack of homogeneity of the **1P1** sample.

A noticeable decrease of the luminescence intensity accompanied by a slight bathochromic shift (av. by 20 nm), a decrease of the band half-width and an increase of the band asymmetry for all complexes under investigation is observed at 77 K. It suggests that the emission is a result of at least two independent processes. The diexponential fitting of the decay curves (eqn (3)) is in an excellent agreement with the experimental decay curves (λ_{ex} = 355 nm). In all cases the slower decay is the dominating one as shown by two parameters shown in Table 2:[6] a population ratio (eqn (4): γ_1) of the emissive state responsible for the slower decay, and an emission yield for the slower decay (eqn (5): R_1).

Table 2 Emission data of **1N–3P3** compounds (excitation: 450 nm)

	r.t.			77 K			
	λ_{em}[a] [nm]	(width; asymmetry)[b]	Lifetimes [μs] τ_1, τ_2 (γ_1, R_1)[c]	λ_{em}[a] [nm]	(width; asymmetry)[b]	Lifetimes [μs] τ_1, τ_2, (γ_1, R_1)[c]	$\Delta\lambda_{em}$[f] [nm]
1N	**593**	(102.758; 0.369)	6.4, 1.7 (0.56, 0.83)	**612**	(90.231; 0.477)	35.5, 4.9 (0.63, 0.93)	19
1N1	**588**	(100.533; 0.387)	7.1, 1.8 (0.60, 0.86)	**611**	(88.723; 0.549)	35.8, 4.8 (0.60, 0.92	25
3N	**590**	(101.507; 0.352)	7.5, 2.2 (0.69, 0.89)	**610**	(91.533; 0.577)	32.6, 4.8 (0.67, 0.93)	20
3N3	**589**	(101.157; 0.388)	6.5, 2.0 (0.70, 0.88)	**606**	(88.516; 0.550)	33.5, 5.4 (0.68, 0.93)	17
4N4	**592**	(101.427; 0.345)	10.0, 2.0 (0.49, 0.83)	**605**	(89.463; 0.533)	47.1, 6.5 (0.66, 0.93)	13
1P	**653**[d]	(142.500; 0.351)	—[e]	**698**[d]	(121.465; 0.423)	—	45
1P1	**642**	(106.476; 0.346)	<1	**657**	(98.966; 0.443)	8.5, 3.1 (0.62, 0.82)	15
3P	**650**[d]	(125.771; 0.454)	—	**685**[d]	(126.508; 0.264)	—	35
3P3	**648**	(110.284; 0.368)	<1	**686**	(110.616; 0.225)	7.5, 1.9 (0.55, 0.83)	38

[a] Uncorrected spectra. [b] Results from fitting the spectrum to the Log-normal curve. [c] Excitation: 355 nm; γ_1 – population ratio of the emissive state responsible for the slower decay, R_1 – emission yield for the slower decay $\Delta\lambda_{em} = \lambda_{em}(77\ K) - \lambda_{em}(r.t.)$. [d] From the previous work[32] (excitation: 470 nm). [e] Not measured. [f] $\Delta\lambda_{em} = \lambda_{em}(77\ K) - \lambda_{em}(r.t.)$

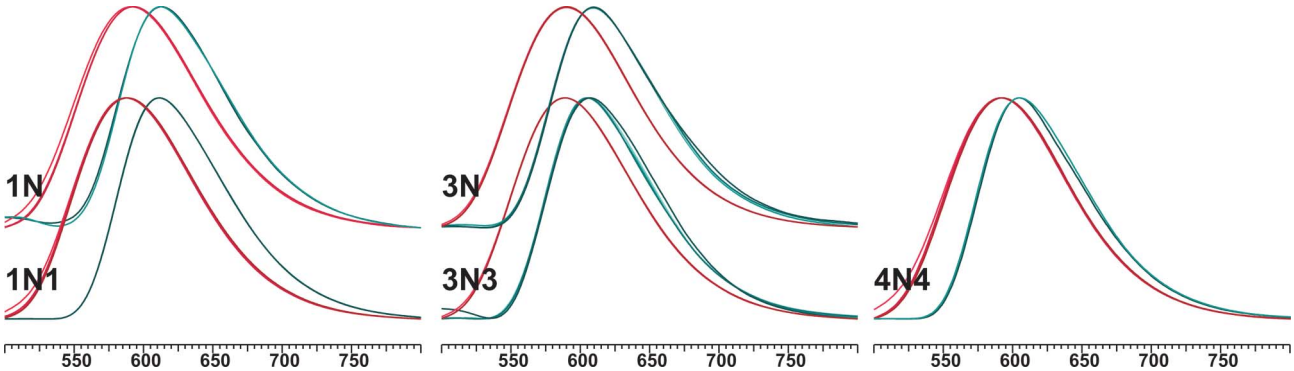

Fig. 5 Uncorrected, normalized emission spectra of the solid ***N*** complexes (λ_{ex} = 450, 360, 325 and 275 nm) Spectra on the left (red) – room temperature; spectra on the right (green) – 77 K.

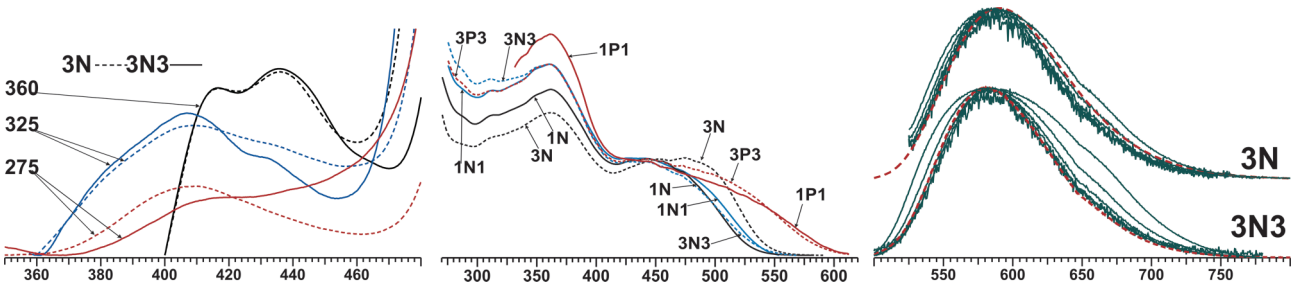

Fig. 6 *Left*: Minor luminescence bands observed at room temperature for **3N** and **3N3** when excited with 360, 325 and 275 nm. (Completely different shape of the bands excited with 360 nm line is the result of a filter used). *Middle*: Corrected excitation spectra measured for maximum of emission. *Right*: Uncorrected time-dependent luminescence spectra (30, 40, 50, 60 and 80 μs) at room temperature for **3N** and **3N3** (dashed lines – steady-state spectra).

$$I = A_1\exp(-t/\tau_1) + A_2\exp(-t/\tau_2) \quad (3)$$

$$\gamma_1 = A_1/(A_1 + A_2) \quad (4)$$

$$R_1 = A_1\tau_1/(A_1\tau_1 + A_2\tau_2) \quad (5)$$

Lifetimes of the slower decay for the ***N*** complexes are relatively long (5–10 μs) at room temperature[5,28] and increase several times at 77 K (32–47 μs).

Time-resolved emission spectra (λ_{ex} = 450 nm) were performed for **3N** and **3N3** (Fig. 6). Surprisingly, they do not confirm the existence of two independent processes. Although there are certain changes in the shape of the bands and a slight shift of the maximum (**3N** – hipsochromic and **3N3** –bathochromic), since **3N** and **3N3** are the same complex these changes can be regarded as random ones.

Excitation with the 360 nm (or shorter) line of all complexes results in the additional, minor emission bands around 400 nm. These bands (shown in Fig. 5. for **3N** and **3N3** as an example) are most likely a result of an excitation of π→π* transition of coordinated dmp or phen ligands.[26] Observed low intensity of these bands may be caused by energy transfer processes or a simple re-absorption of emitted energy. The existence of these bands may be the source of the diexpotential curves of the lifetimes. Energy transfer processes or even simple re-absorption of emitted light could be responsible for the double decay times, thus they only seemingly contradict the possibility of the single transitions in the complexes.

DFT studies

To allow more insight into the structural and electronic properties of the discussed complexes, DFT calculations have been performed at the B3LYP theory level. The singlet ground-state and triplet geometries have been optimized in the gas phase. The key structural data for **1P–4N** is presented in Table 3 (Fig S19† shows the optimized **3N** and **3P**).

The geometries in singlet ground-states ($^1A_1$) obtained with DFT methods slightly differ from the X-ray structures. Systematic deviation of the bond lengths is most noticeable. However, DFT geometries well express the differences in Cu–I and average P–C bond lengths between ***P*** and ***N*** complexes. It is also worth noting that S4 values are in excellent agreement with the values of S4′ for all the complexes.

The most important difference between the calculated and X-ray structures concerns the flattening distortion. The calculated α angle (Fig. 3) values are much closer to 90° for all compounds, which was expected for the isolated molecules.

Optimized geometries of the triplet ($^3A_1$) states significantly differ from the singlet ones. The flattening deformation is larger for the ***P*** complexes (α: 39–47°) than for the ***N*** ones (α: 70–74°). Smaller flattening for **4P** and **4N** is noticeable.

The switch from the $^1A_1$ to $^3A_1$ state involves an increase of the charge on the Cu, P and I atoms. Simultaneously the Cu–P bond is significantly lengthened (by av. 0.14 Å). This should be expected since the electronic properties of copper(I) in the excited triplet state are similar to the properties of copper(II).[1]

In order to determine the type of UV-Vis transitions and get some insight into the luminescence spectra, TDDFT calculations

Table 3 Selected geometries and NBO charges of **1P**, **3P**, **4P**, **1N**, **3N** and **4N**

	1P	3P	4P	1N	3N	4N
$^1A_1$						
d(CuI)	2.6504	2.6337	2.6861	2.6775	2.6490	2.6616
d(CuP)[a]	2.3177	2.3265	2.3241	2.3452	2.3515	2.3609
av. *d*(PC)	1.8745	1.8750	1.8454	1.8826	1.8833	1.8483
I–Cu–P	106.42	105.74	117.05	111.04	110.76	118.79
S4[b]	48.26	49.61	30.38	55.70	56.49	34.28
α (°)	86.90	87.63	89.31	86.34	86.76	86.31
β (°)	142.85	136.27	134.83	145.47	143.24	123.17
γ (°)	110.73	118.00	108.11	103.50	106.02	118.07
q(Cu)	0.75291	0.75427	0.75591	0.75274	0.75394	0.76036
q(I)	–0.79261	–0.78793	–0.78515	–0.79123	–0.78731	–0.78478
q(P)	0.77419	0.76911	0.83409	0.74728	0.74672	0.82897
$^3A_1$						
d(CuI)/Å	2.6845	2.6830	2.6569	2.6713	2.6658	2.6184
d(CuP)/Å[a]	2.4211	2.4240	2.4659	2.4925	2.5017	2.5678
av. *d*(PC)/Å	1.8756	1.8755	1.8402	1.8825	1.8823	1.8423
I–Cu–P (°)	91.10	90.90	95.94	97.97	97.64	99.96
S4[b]	42.28	42.13	25.76	49.79	49.85	28.26
α (°)	40.28	39.92	47.41	70.06	70.63	73.73
β (°)	130.14	132.05	131.86	144.82	142.95	123.89
γ (°)	138.75	137.02	132.18	117.22	119.44	144.82
q(Cu)	1.03188	1.03291	1.03860	1.05066	1.05324	1.06481
q(I)	–0.61184	–0.60853	–0.60080	–0.5794	–0.57791	–0.60119
q(P)	0.83618	0.83277	0.91206	0.7937	0.79244	0.89327

[a] *d*(PC) = 1.8821, 1.8820 and 1.8545 Å for **1**, **3** and **4**, respectively. [b] S4 = 63.7 for **1**, 63.4 for **3** and 40.2 for **4** – ref. 40.

were performed. Table 4 contains the data of the selected transitions and the ESI† (Tables S2–S8 and Fig. S7–S18) contains full TDDFT data.

As expected, the first singlet transition (S_1) for all the compounds is mostly of HOMO → LUMO type. First two intense CT transitions (S_5 and S_6) are dominated by electron transfer from HOMO-2 to LUMO and LUMO+1 orbitals, except **1N** and **3N**: HOMO-2 → LUMO and HOMO-1 → LUMO+1 (S_4 and S_5).

These transitions correspond to the first bands in the absorbance spectra, because their calculated energies are in very good agreement with the maxima of the corresponding bands in the absorbance and excitation spectra, both at the beginning (S_1 edge transition) and the maximum of the bands. An unambiguous difference between the ***P*** and ***N*** complexes is in very good agreement with the experimental data.

Population analysis of molecular orbitals (Fig. 7, also Tables S2–S7† and Fig. S13–S18†) clearly indicates that (for all complexes) the unoccupied orbitals: LUMO and LUMO+1 are dominated by π* orbitals of the diimine ligand. HOMO orbitals are mostly composed of p orbitals of the iodide atom (65–76%) and d orbitals of the Cu atom (11–19%). HOMO-1 orbitals are composed mostly of σ(CuI) bond orbitals and HOMO-2 orbitals are composed of σ(CuI) bond orbitals with a small admixture of the σ(CuP) bond. The complex character of the HOMO and lower orbitals was also observed in many other copper(I) complexes.[1,9,16,17,20,22,25,30,31]

Therefore, the first intense band in the UV-Vis absorption spectra of the **1P–4N** complexes can be unambiguously ascribed to (MX,MPR$_3$)LCT with electron transfer from Cu–I and Cu–P bonds to the antibonding orbitals of the diimine ligand. Ascription of the absorption CT band in [Cu(NCS)(py)$_2$(PPh$_3$)] and [Cu(NCS)(phen)(PPh$_3$)] as MLLCT bands, which involve charge transfer from the metal (with some contribution from NCS ligand) to the py or phen rings[31] supports our analysis.

First triplet transitions (Table 4: T_1) for all the compounds are, like the S_1 transition, mostly of HOMO → LUMO type. Second triplet transition T_2, is more complex than T_1, but in all cases is composed mostly of HOMO-1 → LUMO transition. The differences between the energies of these transitions

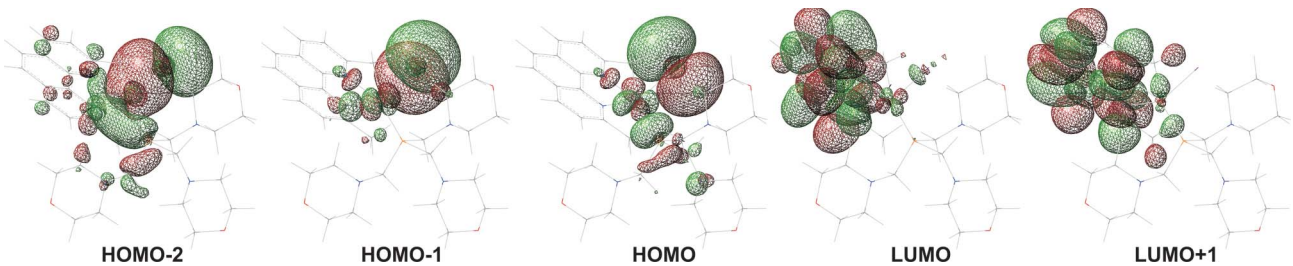

Fig. 7 Molecular orbitals of **3N** calculated with DFT methods. HOMO-2: Cu$^+$ – 37.2; I$^-$ – 47.4; dmp – 6.7; **3** – 8.7%. HOMO-1: Cu$^+$ – 15.7; I$^-$ – 77.2; dmp – 5.7; **3** – 1.4%. HOMO: Cu$^+$ – 18.0; I$^-$ – 69.6; dmp – 1.8; **3** – 10.7%. LUMO: Cu$^+$ – 2.6; I$^-$ – 1.7; dmp – 94.3; **3** – 1.5%. LUMO+1: Cu$^+$ – 0.2; I$^-$ – 0.1; dmp – 99.0; **3** – 0.7%.

Table 4 UV-Vis transitions (in nanometres) from TDDFT calculations

	1P	3P	4P	1N	3N	4N
First triplet transition	T_1: 652.43	T_1: 648.83	T_1:652.70	T_1: 572.23	T_1: 565.52	T_1: 579.74
Transition type:	H→L[a] (84%)[b]	H→L (89%)	H→L (100%)	H→L (95%)	H→L (93%)	H→L (100%)
	H→L1 (8%)	H→L1 (5%)		H1→L (5%)	H1→L (7%)	
First (edge) singlet transition	S_1: 630.85	S_1: 628.66	S_1:635.48	S_1: 564.17	S_1: 557.20	S_1: 569.93
(Oscillator strength)	(0.0064)	(0.0074)	(0.0029)	(0.0021)	(0.0021)	(0.0034)
Transition type:	H→L (87%)	H→L (91%)	H→L (100%)	H→L (100%)	H→L (100%)	H→L (100%)
	H→L1 (9%)	H→L1 (6%)				
Second triplet transition	T_2: 623.39	T_2: 620.83	T_2:619.63	T_2: 557.84	T_2: 551.36	T_2: 554.05
Transition type:	H1→L (69%)	H1→L (79%)	H1→L (82%)	H1→L (75%)	H1→L (79%)	H1→L (94%)
	H1→L1 (18%)	H1→L1 (12%)	H→L1 (15%)	H2→L (18%)	H2→L (11%)	H3→L (4%)
First intense singlet *trans*.	S_5: 555.05	S_5: 545.92	S_5: 523.54	S_4: 506.47	S_4: 499.78	S_5: 485.72
(Oscillator strength)	(0.0257)	(0.0388)	(0.0090)	(0.0274)	(0.0252)	(0.0543)
Transition type:	H2→L (71%)	H2→L (82%)	H2→L (12%)	H2→L (59%)	H2→L (56%)	H2→L (100%)
	H2→L1(29%)	H2→L1(18%)	H2→L1(88%)	H1→L1(41%)	H1→L1(44%)	
Second intense singlet *trans*.	S_6: 549.58	S_6: 541.21	S_6: 520.99	S_5: 501.30	S_5: 495.06	S_6: 467.35
(Oscillator strength)	(0.0470)	(0.0349)	(0.0682)	(0.0353)	(0.0373)	(0.0075)
Transition type:	H2→L (25%)	H2→L (15%)	H2→L (88%)	H2→L (37%)	H2→L (41%)	H2→L1 (100%)
	H2→L1(75%)	H2→L1(85%)	H2→L1(12%)	H1→L1(63%)	H1→L1(59%)	

[a] H – HOMO – highest occupied molecular orbital; L – LUMO – lowest unoccupied molecular orbital; H1, H2 . . . – orbitals of lower energy than HOMO (in descending order); L1, L2 . . . – orbitals of higher energy than LUMO (in ascending order). [b] Most calculated transitions are complex, the percentage is given for dominating participation.

$\lambda(T_1) - \lambda(T_2)$ is equal to 14.4, 14.2 and 25.7 nm for **1N**, **3N**, **4N**, respectively. The analogous difference for ***P*** complexes equals 29.0, 28.0 and 33.1 nm for **1P**, **3P** and **4P**, respectively. These values approximately correspond to the bathochromic shift of the maximum of the emission band accompanying the change of the temperature from r.t. to 77 K.

Summarising, the above analysis suggests that there might be two transitions in thermal equilibrium responsible for the observed excitation-emission processes. T_2 dominates at room temperature and T_1 at 77 K.

Experimental

All reactions were carried out under a dinitrogen atmosphere using standard Schlenk techniques. CuI, PPh_3, phen·H_2O and dmp·0.5H_2O were obtained from Sigma–Aldrich. Phosphines **1** and **3** were synthesized as described previously.[32] All solvents were used without purification; only deaerated prior to use. Elemental analysis was performed with a Vario EL3 CHN analyzer.

Spectroscopic methods

NMR spectra were recorded on a Bruker AMX 300 ($^{13}C\{^1H\}$, $^{31}P\{^1H\}$) spectrometer with traces of solvent as an internal reference for ^1H and ^{13}C ($CDCl_3$ ^1H: δ = 7.27 ppm; ^{13}C: δ = 77.0 ppm) and 85% H_3PO_4 in H_2O as an external standard for ^{31}P. The splitting of proton resonances in the reported ^1H-NMR spectra are defined as s = singlet, d = doublet, t = triplet and m = multiplet. UV-Vis reflectance spectra were recorded on a Cary 5 spectrometer.

Luminescence studies

Luminescence spectra were recorded at room (298 K) and liquid nitrogen (77 K) temperatures using a SpectraPro 750 1-meter monochromator, coupled to a Hamamatsu R928 photomultiplier and equipped with a 1200 l mm^{-1} grating blazed at 500 nm. A 450 W xenon lamp was used as an excitation source. It was coupled to a 275 mm excitation monochromator equipped with a 1800 l mm^{-1} grating blazed at 250 nm. The luminescence decay traces were also recorded at 298 and 77 K, using a Tektronix TDS 3052B oscilloscope and a Nd:YAG Lambda Physics pulsed laser with an excitation line of 355 nm. Time dependent luminescence spectra and excitation spectra were undertaken on a Fluorolog FL 3–22 spectrometer with double gratings for the excitation and emission spectrometer applied as monochromators and a photomultiplier as a detector.

Luminescence spectra (including time-resolved ones) are uncorrected. We decided to show and discuss them in this way due to some artificial effects (random changes of the band shapes and luminescence maxima), which occurred after correction (also appeared in other studies[3]). In general, the weaker the intensity of the spectrum, the larger the shift of the bands to longer wavelengths is observed. Random after-correction changes of the spectra were even observed for the same sample (and excitation wavelength) measured in different positions. These effects can be explained by the fact, that the broad CT band covers almost all the recorded λ range. Thus there are no areas of pure base lines in the spectra, which makes a proper correction almost impossible.

Computational methods

DFT calculations for **1P–4N** complexes were performed using the GAUSSIAN 03 package.[41] For geometry optimizations and the single-point energy calculations we employed the Becke hybrid three parameter DFT method using the Lee, Yang and Parr correlation functional[42] (B3LYP). The basis set employed was 6-31G(d,p) for all atoms, except for iodine atom – 6-311G(d,p)[43] and Cu atom for which the Los Alamos double-ζ (LanL2Dz) basis set was employed with the core potential (Los Alamos ECP), which replaces the inner core electrons. The singlet ground-state structures of all the compounds were optimized in the gas phase starting from corresponding X-ray geometries. Triplet geometries

were also optimized in the gas phase starting from corresponding singlet ground states geometries. Minima of energy were characterized as such by computation of the harmonic vibrational frequencies. For the complexes in the singlet ground states, time-dependent density functional theory[44] (TDDFT) was used to calculate the excited-state energies (the first 60 singlet and 30 first triplet excited-state energies). Charges of atoms in molecules were calculated with a full Natural Bond Orbital analysis, using NBO version 3.[45] The percentage of the atomic/ligand contributions were calculated as $[n^2/\{\mathrm{sum}(n^2)\}]\cdot 100\%$, where n = atomic orbital coefficients in a specific molecular orbital.

Syntheses

All mixtures: **1N1**, **3N3**, **4N4**, **1P1** and **3P3** were prepared by adding an equimolar mixture of solid CuI (0.2–0.3 g) and diimine ligand (dmp or phen) to a solution of two fold molar excess of appropriate phosphine dissolved in 30–40 ml of $CHCl_3$. After 3 h of stirring of the mixture at room temperature, solvent was evaporated under vacuum to dryness. Solid mixtures were then dried at 40 °C under vacuum for several hours. Pure complexes **1N**, **3N** or **4N** were obtained by crystallization of the solution of **1N1**, **3N3** or **4N4**, respectively, in the mixture of CH_2Cl_2 and acetone at −18 °C. Deposited crystalline solids were then filtered and dried at 40 °C under vacuum for several hours. NMR spectra of **1N**, **3N** or **4N** complexes showed no traces of CH_2Cl_2 or acetone. Single crystals for X-ray analysis of $\mathbf{1N}\cdot 0.46(C_6H_{12})\cdot CH_2Cl_2\cdot 2H_2O$ were obtained from **1N1** in the cyclohexane/H_2Cl_2 mixture by slow evaporation of the solvents in air at room temperature. Single crystals of **3N** and $\mathbf{4N}\cdot 2CHCl_3$ complexes were collected from the solutions of **3N3** and **4N4** in the $CHCl_3$/acetone mixtures cooled to −18 °C.

1N: *Anal.* Calcd for $C_{32}H_{51}CuIN_8P$: C, 49.96; H, 6.68; N, 14.57. Found: C, 49.89; H, 6.70; N, 14.54%. **3N**: *Anal.* Calcd for $C_{29}H_{42}CuIN_5O_3P$: C, 47.71; H, 5.80; N, 9.59. Found: C, 47.68; H, 5.83; N, 9.54%. **4N**: *Anal.* Calcd for $C_{32}H_{27}CuIN_2P$: C, 58.15; H, 4.12; N, 4.24. Found: C, 58.13; H, 4.15; N, 4.23%.

NMR ($CDCl_3$, 298 K) {chemical shift [ppm] (multiplicity, coupling constants [Hz])}:

1N1: $^{31}P\{^1H\}$: −29 (s*), −60 (s*); ^1H: dmp: 3.20, 7.58 (d, 8.16) 7.74, 8.20 (d, 8.16); PR_3: 2.20, 2.27, 2.53, 2.73; $^{13}C\{^1H\}$: dmp: 27.65, 124.78, 125.27, 127.00, 136.35, 142.90, 159.08, PR_3: 46.91, 55.02, 54.8–55.1*, 55–58*; ***1N***: $^{31}P\{^1H\}$: −28.5 (s*); ^1H: dmp: 3.20, 7.62 (d, 8.36) 7.77, 8.23 (d, 8.36); PR_3: 2.17, 2.18, 2.52, 2.87; $^{13}C\{^1H\}$: dmp: 27.59, 124.86, 125.33, 127.05, 136.45, 142.94, 159.08, PR_3: 45.79, 54.92, 55.0–55.2*; ***3N3***: $^{31}P\{^1H\}$: −29 (s*), −60 (s*); ^1H: dmp: 3.23, 7.62 (d, 8.32) 7.77, 8.24 (d, 8.32); PR_3: 2.51, 2.77, 3.36; $^{13}C\{^1H\}$: dmp: 27.55, 124.84, 125.36, 127.02, 136.55, 142.79, 159.02, PR_3: 55.47 (d, 6.1), 56.6*, 66.77; ***3N***: $^{31}P\{^1H\}$: −28.5 (s*); ^1H: dmp: 3.24, 7.64 (d, 8.16) 7.79, 8.25 (d, 8.16); PR_3: 2.52, 2.88, 3.38; $^{13}C\{^1H\}$: dmp: 27.60, 124.92, 125.41, 127.09, 136.59, 142.88, 159.14, PR_3: 45.79, 54.92, 55.0–55.2; ***4N4***: $^{31}P\{^1H\}$: −6 (s*), ^1H: dmp: 2.81, 7.43 (d, 8.36) 7.74, 8.16 (d, 8.16); $^{13}C\{^1H\}$: dmp: 26.68*, 124.83, 125.28, 126.96, 136.33, 142.99, 159.31, PR_3: 128.34 (d, 7.7), 129.0*, 133.63 (d, 16.8) 136.29 (d, 6.81); ***4N***: $^{31}P\{^1H\}$: −6 (s*), ^1H: dmp: 2.84, 7.75, 8.16 (d, 8.16); $^{13}C\{^1H\}$: dmp: 26.84, 124.89, 125.29, 127.00, 136.27, 143.09, 159.43, PR_3: 128.21 (d, 9.0), 129.25 (d, 1.2), 133.55 (d, 14.4) 134.24 (d, 28.5).

X-ray crystallography

The data were collected at 100 K using a KM4-CCD diffractometer and graphite-monochromated Mo-Kα (λ = 0.71073 Å) radiation generated from a Diffraction X-ray tube operated at 50kV and 20 mA. The images were indexed, integrated, and scaled using the Oxford Diffraction data reduction package.[46] The structure was solved by direct methods using SHELXS97[47] and refined by the full-matrix least-squares method on all F2 data.[48] Non H atoms were included in the refinement with anisotropic displacement parameters, the H atoms were included from the geometry of the molecules. The data were corrected for absorption.[46]

Crystal/refinement data

$\mathbf{1N}\cdot 0.46(C_6H_{12})\cdot CH_2Cl_2\cdot 2H_2O \equiv C_{35.78}H_{62.56}Cl_2CuIN_8O_2P$, M_r = 929.28, Triclinic, Space Group $P\bar{1}$, a = 9.864(3) Å, b = 12.770(3) Å, c = 17.926(4) Å, α = 101.90(3) β = 95.65(3) γ = 96.09(3)°, V = 2180.1(10) Å^3, D_{calcd}(Z = 2) = 1.416 g cm^{-3}, μ_{Mo} = 1.408 mm^{-1}, specimen: 0.15 × 0.12 × 0.10 mm, T_{min} = 0.816, T_{max} = 0.869, θ_{max} = 25.07°, N_{total} = 25888, N = 7726 (R_{int} = 0.0567), N_0 = 5573, R_1 = 0.0403, wR^2 = 0.0948, S = 1.007, T = 100(2) K; The CH_2Cl_2 molecule shows disorder over six positions. Occupation factors of solvent molecule were refined and finally set as 0.298 0.188 0.355 0.088 0.071. In both water molecules hydrogen atoms are disordered over two positions with occupation factor 0.5.

$\mathbf{3N} \equiv C_{29}H_{42}CuIN_5O_3P$, M_r = 730.10, Monoclinic, Space Group $P2_1/c$, a = 9.818(3) Å, b = 19.049(4) Å, c = 17.201(3) Å, β = 99.53(2)°, V = 3181.4(13) Å^3, D_{calcd}(Z = 4) = 1.524 g cm^{-3}, μ_{Mo} = 1.745 mm^{-1}, specimen: 0.15 × 0.12 × 0.10 mm, T_{min} = 0.778, T_{max} = 0.840, θ_{max} = 25.08°, N_{total} = 36380, N = 5647 (R_{int} = 0.0483), N_0 = 4644, R_1 = 0.0216, wR^2 = 0.0465, S = 1.003, T = 100(2) K.

$\mathbf{4N}\cdot 2CHCl_3 \equiv C_{34}H_{27}Cl_6CuIN_2P$, M_r = 899.71, Monoclinic, Space Group $P2_1/n$, a = 17.873(4) Å, b = 9.582(2) Å, c = 21.537(4) Å, β = 97.73(3)°, V = 3654.9(13) Å^3, D_{calcd}(Z = 4) = 1.635 g cm^{-3}, μ_{Mo} = 1.952 mm^{-1}, specimen: 0.15 × 0.15 × 0.11 mm, T_{min} = 0.754, T_{max} = 0.823, θ_{max} = 30.00°, N_{total} = 10667, N = 10444 (R_{int} = 0.0863), N_0 = 6759, R_1 = 0.0453, wR^2 = 0.0989, S = 0.983, T = 100(2) K.

Conclusions

New CuI complexes with dmp and different phosphines are spectroscopically and crystallographically characterized. The complexes exhibit an intense luminescence with relatively long lifetimes in the solid state. It should be pointed out that the luminescence intensity of the ***N*** complexes is a few orders higher compared to the luminescence of the ***P*** ones. All the ***N*** complexes are air and moisture stable, both in the solid state and in solution. Luminescence properties of **1N** and **3N**, as well of the mixtures: **1N1**, **3N3** and **4N4** were investigated. Such an approach let us avoid some accidental errors, like co-crystallization of other species affecting the spectroscopic properties of the investigated compounds. Including ***P*** complexes presented earlier[32,39] into this work enabled us to carry out a wider analysis of the electronic properties of the complexes of $[CuI(NN)PR_3]$ type.

Optimization of molecular geometries with DFT methods unambiguously indicate the strong influence, also observed in X-ray structures and NMR spectra, of methyl groups at positions

2 and 9 of the dmp rings on the molecular geometries of the whole molecules. Methyl groups are placed close to the copper centre, thus they significantly diminish the space available for larger ligands. The geometries of the phosphines change less upon coordination. The presence of –Me groups also causes a lengthening of the bond between copper and iodide ligand. On the other hand, methyl groups protect the molecules of the complex from significant distortions in the excited states and thus stabilize copper at the first oxidation state, which results in stabilisation of the complexes.

Optimized triplet-states geometries show large flattening deformations for the ***P*** complexes and significantly smaller ones for the ***N*** complexes. Although significant deformations of the geometries in the excited states are not possible in the solid state, calculated deformations quite well follow changes in emission intensities, even a slight difference in the intensities of **4N4** and **1N1** or **3N1**. They are also reflected in the longer lifetimes estimated for **4N4**. This suggests that the optimization of triplet states with DFT methods can be pretty useful in the prediction of luminescence properties of new copper(I) complexes, even in the solid state.

TDDFT calculations show that the first singlet transition (S_1) with a very low oscillator strength for all the compounds is mostly of HOMO → LUMO type and corresponds to the edge of absorption in UV-Vis spectra. The first two intense transitions (dominated by electron transfer from HOMO-2 and HOMO-1 to LUMO and LUMO+1 orbitals) correspond to the maximum of the CT band, which can be ascribed to (MX,MPR_3)LCT with electron transfer from σ(CuI) bond with a small admixture of σ(CuP) bond to antibonding orbitals of the phen or dmp ligand. First triplet transitions (T_1) for all the compounds are, similarly to S_1, mostly of HOMO → LUMO type. Second triplet transitions (T_2) are dominated by HOMO-1 → LUMO transitions. Both are (M,X)LCT type. The difference between T_1 and T_2 transitions can be approximately related to the difference in the emission maxima at room and 77 K temperatures. Thus the luminescence process is dominated by T_2 transition at room temperature and by T_1 at 77 K. This does not explain the significant increase of lifetimes at 77 K, but perhaps short lifetimes at room temperature are caused by molecular oscillations, which are significantly suppressed at 77 K.

The **N** complexes of the aminomethylphosphines exhibit a slightly less intense luminescence than the complex with PPh_3, but they are more stable (despite the greater steric demands) and more soluble in the polar solvents.

At present we have started to work on copper(I) iodide complexes with dmp and other, more diversified, tris(aminomethyl)phosphines. Simultaneously we have started to investigate the properties of the analogous complexes with other halogen (or pseudohalogen) ligands. We hope that these studies will provide sufficient data to elucidate thoroughly the impact of phosphine and halogen ligands on the properties of the copper(I) complexes.

Acknowledgements

Calculations have been carried out in the Wroclaw Centre for Networking and Supercomputing (http://www.wcss.wroc.pl), grant No. 140. The authors are grateful to Prof. Małgorzata Jeżowska-Bojczuk for helpful discussions and her interest in the work.

Notes and references

1 X. Chen, G. B. Shaw, I. Novozhilova, T. Liu, G. Jennings, K. Attenkofer, G. J. Meyer and P. Coppens, *J. Am. Chem. Soc.*, 2003, **125**, 7022–7034.
2 G. Blasse, P. A. Breddels and D. R. McMillin, *Chem. Phys. Lett.*, 1984, **109**, 24–26.
3 D. Felder, J.-F. Nierengarten, F. Barigelletti, B. Ventura and N. Armaroli, *J. Am. Chem. Soc.*, 2001, **123**, 6291–6299.
4 A. Yu. Kovalevsky, M. Gembicky, I. V. Novozhilova and P. Coppens, *Inorg. Chem.*, 2003, **42**, 8794–8802.
5 A. Yu. Kovalevsky, M. Gembicky and P. Coppens, *Inorg. Chem.*, 2004, **43**, 8282–8289.
6 A. Robertazzi, A. Magistrato, P. de Hoog, P. Carloni and J. Reedijk, *Inorg. Chem.*, 2007, **46**, 5873–5881.
7 A. Lavie-Cambot, M. Cantuel, Y. Leydet, G. Jonusauskas, D. M. Bassani and N. D. McClenaghan, *Coord. Chem. Rev.*, 2008, **252**, 2572–2588.
8 M. Iwamura, S. Takeuchi and T. Tahara, *J. Am. Chem. Soc.*, 2007, **129**, 5248–5256.
9 I. I. Vorontsov, T. Graber, A. Yu. Kovalevsky, I. V. Novozhilova, M. Gembicky, Y.-S. Chen and P. Coppens, *J. Am. Chem. Soc.*, 2009, **131**, 6566–6573.
10 G. Blasse and D. R. McMillin, *Chem. Phys. Lett.*, 1980, **70**, 1–3.
11 R. A. Rader, D. R. McMillin, M. T. Buckner, T. G. Matthews, D. J. Casadonte, R. K. Lengel, S. B. Whittaker, L. M. Darmon and F. E. Lytle, *J. Am. Chem. Soc.*, 1981, **103**, 5906–5912.
12 J. R. Kirchhoff, D. R. McMillin, W. R. Robinson, D. R. Powell, A. T. McKenzie and S. Chen, *Inorg. Chem.*, 1985, **24**, 3928–3933.
13 S. Sakaki, H. Mizutani, Y. Kase, K. Inukochi, T. Arai and T. Hamada, *J. Chem. Soc., Dalton Trans.*, 1996, 1909–1914.
14 Y. Sun, S. Zhang, G. Li, Y. Xie and D. Zhao, *Transition Met. Chem.*, 2003, **28**, 772–776.
15 D. Li, R.-Z. Li, Z. Ni, Z-Y. Qi, X.-L. Feng and J.-W. Cai, *Inorg. Chem. Commun.*, 2003, **6**, 469–473.
16 L. Yang, J.-K. Feng, A.-M. Ren, M. Zhang, Y.-G. Ma and X.-D. Liu, *Eur. J. Inorg. Chem.*, 2005, 1867–1879.
17 T. McCormic, W.-L. Jia and S. Wang, *Inorg. Chem.*, 2006, **45**, 147–155.
18 O. Moudam, A. Kaeser, B. Dalavoux-Nicot, C. Duhayon, M. Holler, G. Accorsi, I. Séguy, P. Destruel and J.-F. Nierengarten, *Chem. Commun.*, 2007, 3077–3079.
19 N. Armaroli, G. Accorsi, G. Bergamini, P. Ceroni, M. Holler, O. Moudam, C. Duhayon, B. Delavaux-Nicot and J.-F. Nierengarten, *Inorg. Chim. Acta*, 2007, **360**, 1032–1042.
20 W. F. Fu, X. Gan, J. Jiao, Y. Chen, M. Yuan, S.-M. Chi, M.-M. Yu and S.-X. Xiong, *Inorg. Chim. Acta*, 2007, **360**, 2758–2766.
21 A. Listorti, G. Accorsi, Y. Rio, N. Armaroli, O. Moudam, A. Gégout, B. Delavaux-Nicot, M. Holler and J. F. Nierengarten, *Inorg. Chem.*, 2008, **47**, 6254–6261.
22 L. Zhang, B. Li and Z. Su, *J. Phys. Chem. C*, 2009, **113**, 13968–13973.
23 L. Zhang, B. Li and Z. Su, *Langmuir*, 2009, **25**, 2068–2074.
24 S. Kabehie, A. Z. Stieg, M. Xue, M. Liong, K. L. Wang and J. I. Zink, *J. Phys. Chem. Lett.*, 2010, **1**, 589–593.
25 Y. Chen, J.-S. Chen, X. Gan and W.-F. Fu, *Inorg. Chim. Acta*, 2009, **362**, 2492–2498.
26 R. K. Reigle, D. J. Casadonte, Jr. and S. G. Bott, *J. Chem. Crystallogr.*, 1994, **24**, 769–773.
27 A. Dairiki, T. Tsukuda, K. Matsumoto and T. Tsubomura, *Polyhedron*, 2009, **28**, 2730–2734.
28 Y.-J. Shi, S.-J. Chen, B. Huang, X.-T. Chen, Y. Zhang and X.-Z. You, *J. Mol. Struct.*, 2003, **650**, 27–32.
29 A. Tsuboyama, K. Kuge, M. Furugori, S. Okada, M. Hoshino and K. Ueno, *Inorg. Chem.*, 2007, **46**, 1992–2001.
30 X. Gan, W.-F. Fu, Y.-Y. Lin, M. Yuan, C.-M. Che, S.-M. Chi, H.-F. J. Li, J.-H. Chen and Z.-Y. Zhou, *Polyhedron*, 2008, **27**, 2202–2208.
31 C. Pettinari, C. di Nicola, F. Marchetti, R. Pettinari, B. W. Skelton, N. Somers, A. H. White, W. T. Robinson, M. R. Chierotti, R. Gobetto and C. Nervi, *Eur. J. Inorg. Chem.*, 2008, 1974–1984.
32 R. Starosta, M. Florek, J. Król, M. Puchalska and A. Kochel, *New J. Chem.*, 2010, **34**, 1441–1449.
33 R. Starosta, B. Bażanów and W. Barszczewski, *Dalton Trans.*, 2010, **39**, 7547–7555.
34 C. A. Tolman, *J. Am. Chem. Soc.*, 1970, **92**, 2956–2965; C. A. Tolman, *Chem. Rev.*, 1977, **77**, 313–348.
35 B. J. Dunne, R. B. Morris and A. G. J. Orpen, *J. Chem. Soc., Dalton Trans.*, 1991, 653–661.

36 J. Mathew, T. Thomas and C. H. Suresh, *Inorg. Chem.*, 2007, **46**, 10800–10809.
37 C. H. Suresh and N. Koga, *Inorg. Chem.*, 2002, **41**, 1573–1578.
38 C. H. Suresh, *Inorg. Chem.*, 2006, **45**, 4982–4986.
39 Q.-H. Jin, X.-L. Xin, Ch.-J. Dong and H.-J. Zhu, *Acta Crystallogr., Sect. C: Cryst. Struct. Commun.*, 1998, **54**, 1087–1089.
40 B. J. Dunne and A. G. Orpen, *Acta Crystallogr., Sect. C: Cryst. Struct. Commun.*, 1991, **C47**, 345–347.
41 *Gaussian 03, Revision D.01*, M. J. Frisch, G. W. Trucks, H. B. Schlegel, G. E. Scuseria, M. A. Robb, J. R. Cheeseman, J. A. Montgomery, Jr., T. Vreven, K. N. Kudin, J. C. Burant, J. M. Millam, S. S. Iyengar, J. Tomasi, V. Barone, B. Mennucci, M. Cossi, G. Scalmani, N. Rega, G. A. Petersson, H. Nakatsuji, M. Hada, M. Ehara, K. Toyota, R. Fukuda, J. Hasegawa, M. Ishida, T. Nakajima, Y. Honda, O. Kitao, H. Nakai, M. Klene, X. Li, J. E. Knox, H. P. Hratchian, J. B. Cross, V. Bakken, C. Adamo, J. Jaramillo, R. Gomperts, R. E. Stratmann, O. Yazyev, A. J. Austin, R. Cammi, C. Pomelli, J. W. Ochterski, P. Y. Ayala, K. Morokuma, G. A. Voth, P. Salvador, J. J. Dannenberg, V. G. Zakrzewski, S. Dapprich, A. D. Daniels, M. C. Strain, O. Farkas, D. K. Malick, A. D. Rabuck, K. Raghavachari, J. B. Foresman, J. V. Ortiz, Q. Cui, A. G. Baboul, S. Clifford, J. Cioslowski, B. B. Stefanov, G. Liu, A. Liashenko, P. Piskorz, I. Komaromi, R. L. Martin, D. J. Fox, T. Keith, M. A. Al-Laham, C. Y. Peng, A. Nanayakkara, M. Challacombe, P. M. W. Gill, B. Johnson, W. Chen, M. W. Wong, C. Gonzalez, and J. A. Pople, Gaussian, Inc., Wallingford CT, 2004.
42 A. D. Becke, *Phys. Rev. A: At., Mol., Opt. Phys.*, 1988, **38**, 3098; A. D. Becke, *J. Chem. Phys.*, 1993, **98**, 5648; C. Lee, W. Yang and R. G. Parr, *Phys. Rev. B*, 1988, **37**, 785.
43 EMSL Basis Set Exchange Library https://bse.pnl.gov/bse/portal, M. N. Glukhovstev, A. Pross, M. P. McGrath and L. Radom, *J. Chem. Phys.*, 1995, **103**, 1878.
44 R. E. Stratmann, G. E. Scuseria and M. J. Frisch, *J. Chem. Phys.*, 1998, **109**, 8218; R. Bauernschmitt and R. Ahlrichs, *Chem. Phys. Lett.*, 1996, **256**, 454; M. E. Casida, C. Jamorski, K. C. Casida and D. R. Salahub, *J. Chem. Phys.*, 1998, **108**, 4439.
45 J. E. Carpenter and F. Weinhold, *THEOCHEM*, 1988, **169**, 41; J. E. Carpenter, *PhD thesis*, University of Wisconsin, Madison, WI, 1987; J. P. Foster and F. Weinhold, *J. Am. Chem. Soc.*, 1980, **102**, 7211; A. E. Reed and F. Weinhold, *J. Chem. Phys.*, 1983, **78**, 4066; A. E. Reed and F. Weinhold, *J. Chem. Phys.*, 1983, 1736; E. Reed, R. B. Weinstock and F. Weinhold, *J. Chem. Phys.*, 1985, **83**, 735; A. E. Reed, L. A. Curtiss and F. Weinhold, *Chem. Rev.*, 1988, **88**, 899; F. Weinhold and J. E. Carpenter, *Plenum*, 1988, 227.
46 Oxford Diffraction Poland Sp., CCD data collection and reduction GUI, Version 1.173.13 beta (release 14.11.2003), Copyright 1995–2003.
47 G. M. Sheldrick, *SHELXS97 Program for Solution of Crystal Structure*, University of Goettingen, Germany, 1997. Release 97-2.
48 G. M. Sheldrick, *SHELXl97 Program for Refinement of Crystal Structure*, University of Goettingen, Germany, 1997.

